Coupled Systems Mechanics, *Vol. 15, No. 2 (2026) 135-155*
https://doi.org/10.12989/csm.2026.15.2.135

Techno-Press

Mechanical and thermal buckling analysis of P-FG plate using an innovative HSDT and Airy stress function

Ahmed Bakoura*[1,2], Aicha Remil[3], Aicha Bessaim[2,3], Mohammed Sid Ahmed Houari[3], Sahla Meriem[3], Ibka Mohamed Soufiane[4], Abdelouahed Tounsi[1]

[1]*Material and Hydrology Laboratory, Civil Engineering Department, Faculty of Technology, University of Sidi Bel Abbes, Algeria*
[2]*Département de Génie Civil, Faculté d'Architecture et de Génie Civil, Université des Sciences et de la Technologie d'Oran, BP 1505 El M'naouer, USTO, Oran, Algeria*
[3]*Laboratoire d'Etude des Structures et de Mécanique des Matériaux, Département de Génie Civil, Faculté des Sciences et de la Technologie, Université Mustapha Stambouli, B.P. 305, R.P. 29000 Mascara, Algeria*
[4]*Laboratoire Signaux et Images (LSI), University of Science and Technology of Oran, Mohammed Boudiaf, Bir El Djir 31000, Algeria*

(Received January 19, 2026, Revised April 12, 2026, Accepted April 14, 2026)

Abstract. In this article, the mechanical and thermal buckling analysis of simply-supported functionally graded plates resting on an elastic foundation is conducted using an innovative higher shear deformation theory (HSDT) in conjunction with the Airy stress function method. The key novelty of this work lies in the exact resolution of the equilibrium equations through the Airy stress function, eliminating the need for shear correction factors, and in the introduction of a new transverse shear function that ensures a parabolic variation of transverse shear stresses across the thickness while naturally satisfying the stress-free boundary conditions at the surfaces. Three types of thermal loads are considered: uniform, linear, and nonlinear distributions through the thickness. The material properties of the plate vary according to a power-law distribution based on the volume fraction of its constituents. Numerical results are presented to assess the effects of the power-law index the foundation stiffness and geometric ratios on the critical buckling load and the critical buckling temperature, highlighting the accuracy and efficiency of the proposed methodology.

Keywords: airy stress function; analytical modeling; buckling; computational modeling; functionally graded plate; refined plate theory

1. Introduction

Functionally graded materials (FGMs) embody a sophisticated class of composites characterized by a continuous, spatially varying distribution of properties such as mechanical strength, thermal conductivity, and stiffness across their thickness. This gradual transition distinguishes FGMs from conventional laminated composites, mitigating abrupt property discontinuities that often lead to stress concentrations and compromised interfacial integrity [1-5]. These attributes render FGMs particularly advantageous for high-performance applications,

*Corresponding author, Ph.D., E-mail: bakoura.ahmed@outlook.fr

ISSN: 2234-2184 (Print), 2234-2192 (Online)

including aerospace, biomedical implants, and automotive systems, where exceptional mechanical reliability and thermal resilience are paramount. However, structural components fabricated from FGMs frequently encounter severe environmental conditions, such as elevated temperatures and prolonged moisture exposure, which can profoundly influence their stiffness and long-term durability. Functionally graded materials (FGMs) were initially developed as thermal barrier materials for fusion reactors and aerospace structures, where extreme temperatures and significant thermal gradients are present. Consequently, the thermal response of these structures has attracted considerable attention.

Nowadays, functionally graded materials (FGMs) are widely used in various engineering applications, including nuclear, mechanical, and civil engineering. Consequently, accurately modeling their structural responses under different types of loading using plate, beam, and shell theories is of paramount importance. Over recent years, extensive research has been conducted on the bending, vibration, thermomechanical, and buckling behavior of functionally graded structural elements [6-13]. Considerable effort has been directed toward understanding the static, dynamic, and buckling responses of advanced composite structures subjected to diverse loading and boundary conditions. Such investigations underscore the increasing prominence of FGMs in engineering design, driven by their capacity to alleviate stress concentrations while optimizing mechanical performance. The continuous gradation of constituent materials in FGMs yields enhanced stiffness-to-weight ratios, superior resistance to thermal and mechanical stresses, and improved durability relative to traditional laminates. Consequently, elucidating their response to a spectrum of physical and environmental factors remains a pivotal focus for advancing the development of next-generation composite systems. As a result, a wide range of plate theories has been developed to enhance the accuracy of mechanical response predictions. These theories are generally classified into three main categories: classical plate theory (CPT), first-order shear deformation theory (FSDT), and higher-order shear deformation theory (HSDT) [14-23]. The Classical Plate Theory (CPT) neglects the transverse shear deformation effect, making it suitable only for analyzing thin plates where this effect is insignificant. In contrast, the First-Order Shear Deformation Theory (FSDT) accounts for transverse shear deformation, allowing its application to both thin and moderately thick plates. However, it requires an appropriate shear correction factor to accurately capture the transverse shear stress distribution. To eliminate the need for such correction factors, Higher-Order Shear Deformation Theories (HSDTs) have been developed. These theories, based on either a three-dimensional approach or a two-dimensional formulation with a nonlinear axial displacement variation, provide a parabolic distribution of transverse shear strains through the plate thickness [24]. Therefore, this theory has been increasingly used to predict the behavior of functionally graded plates, as it enhances the accuracy of numerical evaluations for both moderately thick and very thick plates [25]. Extensive research has been conducted on the thermal and mechanical buckling behavior of functionally graded plates resting on elastic foundations. Various plate theories have been employed to improve prediction accuracy and gain deeper insights into the structural response under diverse loading conditions and boundary constraints. Researchers have utilized analytical, numerical, and computational approaches to examine the effects of material gradation, foundation stiffness, and thermal influences on the buckling characteristics of these advanced composite structures. According to the classical plate theory, the thermal critical buckling load is higher than the values reported in other higher-order shear deformation theories. Javaheri and Eslami [26] formulated the equilibrium equations of an FGM plate under thermal loads using a higher-order plate theory. They then obtained analytical solutions for the buckling analysis. Shariat and Eslami [27] developed a

closed-form solution for the critical buckling loads of imperfect rectangular functionally graded material (FGM) plates using Classical Plate Theory (CPT). Kazerouni et al. [28] conducted a thermal buckling analysis of thin functionally graded plates subjected to two types of thermal loading: uniform and nonlinear temperature rise. Kiani et al. [29] derived analytical solutions for the thermal buckling of fully clamped thin functionally graded material (FGM) plates resting on elastic foundations. Their study employed three approximate analytical methods to examine the effects of various thermal loading conditions. Xing and Wang [30] analyzed the thermal buckling behavior of rectangular functionally graded material (FGM) plates under various boundary conditions using the separation-of-variables method. Their study provided valuable insights into the stability of FGM plates subjected to thermal loads. Regarding Isogeometric Analysis (IGA) and in-plane functionally graded (FG) plates, Sitli et al. [31] developed a finite element model to analyze the buckling and post-buckling behavior of functionally graded material (FGM) plates, providing insights into their structural stability under various loading conditions. Using a modified FSDT-based four-node finite shell element, Trabelsi et al. [32] investigated the thermal buckling behavior of FGM plates and shells. Fekrar et al. [33] conducted a buckling analysis of a ceramic-based FGM plate using a four-variable refined theory, demonstrating the accuracy and effectiveness of this mathematical approach in analyzing buckling behavior. Kettaf et al. [34] analyzed the buckling response of FG sandwich plates by considering constant, linear, and nonlinear temperature distributions through the thickness. Zenkour and Aljadani [35] analyzed the buckling of FG plates while considering the thickness stretching effect. Shanab et al. [36] investigated the buckling behavior of bi-directional FG porous plates resting on an elastic foundation using a neutral axis-based model. They analyzed the effects of shear functions, porosity models, and boundary conditions on buckling stability. Li et al. [37] conducted a nonlinear thermal post-buckling analysis of graphene platelets reinforced metal foam plates, considering initial geometrical imperfections. They examined the effects of material properties and graphene distribution patterns on thermal post-buckling strength. Tamrabet et al. [38] analyzed the buckling behavior of FG porous sandwich plates with metallic foam cores on an elastic foundation. They investigated the effects of porosity distribution, boundary conditions, and in-plane loads using a quasi-3D shear deformation theory. Lekouara et al. [39] conducted a theoretical thermal buckling analysis of thick FG porous plates under various boundary conditions and thermal gradients. Using a refined higher-order shear deformation theory, they examined the effects of porosity, foundation parameters, and aspect ratios on critical buckling temperature. Hadji et al. [40] analyzed the thermal buckling of FG plates using a trigonometric shear deformation theory with temperature-dependent material properties. They investigated the effects of grading indices and geometric parameters under various thermal loading conditions. Gao et al. [41] extended the simple refined plate theory (S-RPT) to analyze the bending and buckling of FG-GPLRC plates on local elastic foundations. Their approach simplifies foundation positioning and captures the interplay between material gradients and displacement distribution. Gholami et al. [42] investigated the buckling and postbuckling behavior of sandwich FG-GPLRC porous plates using a higher-order shear deformation model. Their study explores the effects of geometric parameters, porosity, GPL distribution, and boundary conditions on structural stability. Aljadani [43] employed a Quasi-3D theory to analyze the thermal buckling behavior of FG porous plates. The study emphasizes the impact of different porosity distributions and thermal loading conditions on the critical buckling load, providing insights into optimal FGM design considerations. Chenafi et al. [44] introduced a novel strain-based approach incorporating a sinusoidal high-order shear deformation theory to analyze the static and buckling behavior of functionally graded plates. The proposed method

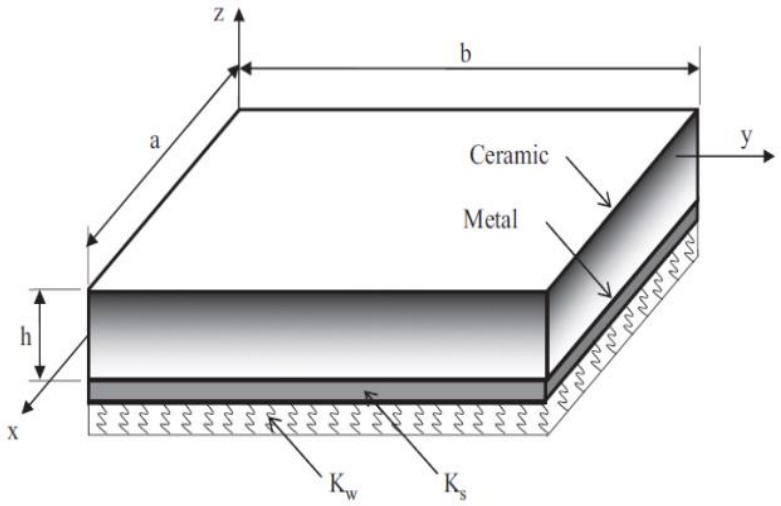

Figure. 1 P-FG plate geometry and coordinates

reduces the number of unknowns while ensuring accurate results, making it a valuable tool for aerospace, automotive, and civil engineering applications.

In this paper, a novel approach combining an advanced higher order shear deformation theory (HSDT) with the Airy stress function method is proposed to analyze the mechanical and thermal buckling of rectangular FG plates. The proposed formulation is variationally consistent, inherently accounts for a parabolic distribution of transverse shear stresses through the thickness, and naturally satisfies the shear stress free boundary conditions, eliminating the need for a shear correction factor. The material properties of the plate are assumed to vary across the thickness following a simple power law distribution based on the volume fraction of its constituents. Numerical results are presented to examine the effects of the power law index and geometric ratios on the critical mechanical and thermal buckling loads.

2. Mechanics of material for the FG plate

Fig. 1 shows the geometry and coordinate system for the functionally graded plate (FGP) resting on elastic foundation. The plate is described by its length (a), breadth (b), and thickness (h), which are the primary geometric dimensions of the rectangular plate.

In this study, the material properties of the FG plate are assumed to follow a mixture rule, as described by [45]. A simple power-law distribution is considered, transitioning from pure metal at the lower surface ($z = -h/2$) to pure ceramic at the upper surface ($z = +h/2$), based on the volume fractions of the constituents [46]. The mechanical and thermal properties of FGMs are derived from the material volume fractions. Specifically, the elastic modulus (E), thermal conductivity (K), coefficient of thermal expansion (α), and Poisson's ratio (ν) are determined by [47-49]

$$E(z) = E_M + \left(E_C - E_M\right)\left(\frac{2z+h}{2h}\right)^N \tag{1a}$$

$$K(z) = K_M + \left(K_C - K_M\right)\left(\frac{2z+h}{2h}\right)^N \tag{1b}$$

$$\alpha(z) = \alpha_M + \left(\alpha_C - \alpha_M\right)\left(\frac{2z+h}{2h}\right)^N, \quad \nu(z) = \nu = \text{constant} \tag{1c}$$

Where N is the gradient index and subscripts M and C denote the metallic and ceramic components, respectively. The value of N equal to zero and infinity represents a fully ceramic and metal plate, respectively.

3. Theory and approximation of FG plate

3.1 Kinematics

In this work, a novel hyperbolic shear deformation plate theory is fitted and proposed. The displacement field can then be expressed as [50]:

$$\begin{aligned} u(x,y,z) &= u_0(x,y) - z\,w_{0,x}(x,y) + \Psi(z)\,\varphi_{,x}(x,y) \\ v(x,y,z) &= v_0(x,y) - z\,w_{0,y}(x,y) + \Psi(z)\,\varphi_{,y}(x,y) \\ w(x,y,z) &= w_0(x,z) \end{aligned} \tag{2a}$$

With

$$\Psi(z) = \frac{\left(1+2e+e^2\right)h\tanh\left(z/h\right)+4ez}{\left(1-2e+e^2\right)} \tag{2b}$$

In this work, a novel hyperbolic shear deformation plate theory is proposed. The transverse shear function in Eq. (2b) has been developed by Professor Mohammed Sid Ahmed Houari and is used here for the first time.

Where u_0, v_0 and w_0 are generalized displacement at the mid-plane of the plate in the x, y, and z directions, respectively; ϕ is the rotations and h is the plate thickness.

The non-linear Von Karman strain-displacement equations are as follows [50]:

$$\begin{pmatrix} \varepsilon_x \\ \varepsilon_y \\ \gamma_{xy} \end{pmatrix} = \begin{pmatrix} \varepsilon_x^0 \\ \varepsilon_y^0 \\ \gamma_{xy}^0 \end{pmatrix} + z\begin{pmatrix} k_x^b \\ k_y^b \\ k_{xy}^b \end{pmatrix} + \Psi(z)\begin{pmatrix} k_x^s \\ k_y^s \\ k_{xy}^s \end{pmatrix}, \quad \begin{Bmatrix} \gamma_{xz} \\ \gamma_{yz} \end{Bmatrix} = \Psi'(z)\begin{Bmatrix} \gamma_{xz}^0 \\ \gamma_{yz}^0 \end{Bmatrix}, \tag{3}$$

Where

$$\begin{Bmatrix} \varepsilon_x^0 \\ \varepsilon_y^0 \\ \gamma_{xy}^0 \end{Bmatrix} = \begin{Bmatrix} u_{0,x} + (w_{0,x})^2/2 \\ v_{0,x} + (w_{0,y})^2/2 \\ u_{0,y} + v_{0,x} + w_{0,x}w_{0,y} \end{Bmatrix}, \begin{Bmatrix} k_x^b \\ k_y^b \\ k_{xy}^b \end{Bmatrix} = \begin{Bmatrix} -w_{0,xx} \\ -w_{0,yy} \\ -2w_{0,xy} \end{Bmatrix}, \begin{Bmatrix} k_x^s \\ k_y^s \\ k_{xy}^s \end{Bmatrix} = \begin{Bmatrix} -\varphi_{,xx} \\ -\varphi_{,yy} \\ -2\varphi_{,xy} \end{Bmatrix}, \begin{Bmatrix} \gamma_{xz}^0 \\ \gamma_{yz}^0 \end{Bmatrix} = \begin{Bmatrix} \varphi_{,x} \\ \varphi_{,y} \end{Bmatrix} \tag{4}$$

3.2 Constitutive equations

The linear constitutive relations of a FG plate can be written as [2]:

$$\begin{Bmatrix} \sigma_x \\ \sigma_y \\ \tau_{xy} \\ \tau_{yz} \\ \tau_{xz} \end{Bmatrix} = \frac{E}{1-\nu^2} \begin{bmatrix} 1 & \nu & 0 & 0 & 0 \\ \nu & 1 & 0 & 0 & 0 \\ 0 & 0 & \frac{1-\nu}{2} & 0 & 0 \\ 0 & 0 & 0 & \frac{1-\nu}{2} & 0 \\ 0 & 0 & 0 & 0 & \frac{1-\nu}{2} \end{bmatrix} \begin{Bmatrix} \varepsilon_x - \alpha\,\Delta T \\ \varepsilon_y - \alpha\,\Delta T \\ \gamma_{xy} \\ \gamma_{yz} \\ \gamma_{xz} \end{Bmatrix} \tag{5}$$

Where ΔT is temperature rise from stress free initial state or temperature difference between two surfaces of the FG plate.

By using the principle of minimum total potential energy, the expressions for the nonlinear equilibrium equations of the plate are obtained as

$$N_{x,x} + N_{xy,y} = 0 \tag{6a}$$

$$N_{xy,x} + N_{y,y} = 0 \tag{6b}$$

$$(M^b_{x,xx} + 2\,M^b_{xy,xy} + M^b_{y,yy}) + N_x w_{,xx} + 2\,N_{xy} w_{,xy} + N_y w_{,yy} - k_w w + k_s \nabla^2 w = 0 \tag{6c}$$

$$M^s_{x,xx} + 2M^s_{xy,xy} + M^s_{y,yy} + Q_{x,x} + Q_{y,y} = 0 \tag{6d}$$

The force and moment resultants (N,Q,S and M) of the FG plate are obtained by

$$(N_i,\ M_i,\ S_i) = \int_{-h/2}^{h/2} \sigma_i\,(1, z, \Psi(z))\,dz, \quad (i = x, y, xy) \tag{7a}$$

$$Q_i = \int_{-h/2}^{h/2} \sigma_j\,\Psi'(z)\,dz, \qquad (i = x, y);\ \ (j = xz, yz) \tag{7b}$$

Substitution of Eqs. (3) and (5) into Eq. (7) yields the constitutive relations as

$$\begin{aligned}(N_x, M^b_x, M^s_x) = \frac{1}{1-\nu^2}[&(E_1, E_2, E_3)\ (\varepsilon^0_x + \nu\,\varepsilon^0_y) + (E_2, E_4, E_5)\ (k^b_x + \nu\,k^b_y) + (E_3, E_5, E_7)\ (k^s_x + \nu\,k^s_y) \\ &-(1+\nu)\ (\Phi_1, \Phi_2, \Phi_3)]\end{aligned} \tag{8a}$$

$$\begin{aligned}(N_y, M^b_y, M^s_y) = \frac{1}{1-\nu^2}[&(E_1, E_2, E_3)\ (\varepsilon^0_y + \nu\varepsilon^0_x) + (E_2, E_4, E_5)\ (k^b_y + \nu\,k^b_x) + (E_3, E_5, E_7)\ (k^s_y + \nu\,k^s_x) \\ &-(1+\nu)\ (\Phi_1, \Phi_2, \Phi_3)]\end{aligned} \tag{8b}$$

$$(N_{xy}, M^b_{xy}, M^s_{xy}) = \frac{1}{2(1+\nu)}[(E_1, E_2, E_3)\ \gamma^0_{xy} + (E_2, E_4, E_5)\ k^b_{xy} + (E_3, E_5, E_7)\ k^s_{xy}] \tag{8c}$$

$$(Q_x, Q_y) = \frac{1}{2(1+\nu)} E_8\left(\gamma_{xz}^0, \gamma_{yz}^0\right) \tag{8d}$$

Where

$$\left(E_1, E_4, E_5, E_7\right) = \int_{-h/2}^{h/2} \left(1, z^2, z\,\Psi(z), \Psi(z)^2\right) E(z) dz, \left(E_2, E_3\right) = \int_{-h/2}^{h/2} \left(z, \Psi(z)\right) E(z) dz, E_8 = \int_{-h/2}^{h/2} \left(\Psi'(z)\right)^2 E(z)\, dz \tag{9a}$$

$$(\Phi_1, \Phi_2, \Phi_3) = \int_{-h/2}^{h/2} (1, z, \Psi) E(z)\, \alpha(z)\, \Delta T(z)\, dz \tag{9b}$$

The last two equations of Eq. (6) may be rewritten into one equation in terms of variables w_0 by substituting Eqs. (4) and (8) into Eqs. (6c)-(6d). Subsequently, elimination of the variable φ from two the resulting equations lead to the following system of equilibrium equations

$$N_{x,x} + N_{xy,y} = 0 \tag{10a}$$

$$N_{xy,x} + N_{y,y} = 0 \tag{10b}$$

$$\begin{aligned}&(D_1 D_3 - D_2^2)\nabla^6 w - D_1 D_4\ \nabla^4 w - D_3 \nabla^2 (N_x w_{,xx} + 2N_{xy} w_{,xy} + N_y w_{,yy} - k_w w + k_s \nabla^2 w) \\ &+ D_4 (N_x w_{,xx} + 2N_{xy} w_{,xy} + N_y w_{,yy} - k_w w + k_s \nabla^2 w) = 0\end{aligned} \tag{10c}$$

Where

$$D_1 = \frac{E_1 E_4 - E_2^2}{E_1(1-\nu^2)}, \quad D_2 = \frac{E_1 E_5 - E_2 E_3}{E_1(1-\nu^2)}, \quad D_3 = \frac{E_1 E_7 - E_3^2}{E_1(1-\nu^2)}, \quad D_4 = \frac{E_8}{2(1+\nu)} \tag{11}$$

For a FG plate, Eq. (10) are modified into form as

$$\begin{aligned}&(D_1 D_3 - D_2^2)\nabla^6 w - D_1 D_4 \nabla^4 w - D_3 \nabla^2 [f_{,yy}(w_{,xx}) - 2\ f_{,xy}(w_{,xy}) + f_{,xx}(w_{,yy}) - k_w w + k_s \nabla^2 w] \\ &+ D_4 [f_{,yy}(w_{,xx}) - 2\ f_{,xy}(w_{,xy}) + f_{,xx}(w_{,yy}) - k_w w + k_s \nabla^2 w] = 0\end{aligned} \tag{12}$$

Where $f(x, y)$ is stress function defined by

$$N_x = f_{,yy}\ ,\ N_y = f_{,xx}\ ,\ N_{xy} = -f_{,xy} \tag{13}$$

The geometrical compatibility equation for a FG plate is expressed as

$$\varepsilon_{x,yy}^0 + \varepsilon_{y,xx}^0 - \gamma_{xy,xy}^0 = w_{,xy}^2 - w_{,xx} w_{,yy} \tag{14}$$

From the constitutive relations (8) and Eq. (13) one can write

$$\begin{aligned}&(\varepsilon_x^0, \varepsilon_y^0) = \frac{1}{E_1}[(f_{,yy}, f_{,xx}) - \nu(f_{,xx}, f_{,yy}) - E_2(k_x^b, k_y^b) - E_3(k_x^s, k_y^s) + \Phi_1(1,1)] \\ &\gamma_{xy}^0 = -\frac{1}{E_1}[2(1+\nu)\ f_{,xy} + E_2\, k_{xy}^s + E_3\, k_{xy}^b]\end{aligned} \tag{15}$$

Introducing Eq. (15) into Eq. (14), the compatibility equation of a FG plate becomes

$$\nabla^4 f - E_1 (w_{0,xy}^2 - w_{0,xx} w_{0,yy}) = 0 \tag{16}$$

In this study we are concerned with the exact solution of Eqs. (12) and (16) for a simply supported FG plate. In this case, the proposed solutions of w and f respecting boundary conditions are assumed to be [51, 52]

$$w = W \sin(\lambda_m x) \sin(\delta_n y) \tag{17a}$$

$$f = A_1 \cos(2\lambda_m x) + A_2 \cos(2\delta_n y) + A_3 \sin(\lambda_m x) \sin(\delta_n y) + \frac{1}{2} N_{x0} y^2 + \frac{1}{2} N_{y0} x^2 \tag{17b}$$

Where $\lambda_m = m\pi/a$, $\delta_n = n\pi/b$, m, n are odd numbers and W is amplitude of the deflection. The coefficients A_i (i=1, 2, 3) are determined by substitution of Eqs. (17a), (17b) into Eq. (16) as

$$A_1 = \frac{E_1 \delta_n^2}{32 \lambda_m^2} W^2, \quad A_2 = \frac{E_1 \lambda_m^2}{32 \delta_n^2} W^2, \quad A_3 = 0 \tag{18}$$

Then, setting Eqs. (17a), (17b) into Eq. (12) and by employing the Galerkin method for the resulting equation yield

$$\begin{aligned} &((D_1 D_3 - D_2^2)(\lambda_m^2 + \delta_n^2)^3 + D_1 D_4 (\lambda_m^2 + \delta_n^2)^2 + [k_w + k_s (\lambda_m^2 + \delta_n^2)][(D_3 (\lambda_m^2 + \delta_n^2) + D_4]) W \\ &+ \frac{E_1}{16} (D_3 (\lambda_m^4 \delta_n^2 + \lambda_m^2 \delta_n^4 + \lambda_m^6 + \delta_n^6) + D_4 (\lambda_m^4 + \delta_n^4)) \times W^3 \\ &+ (D_3 (\lambda_m^2 + \delta_n^2) + D_4) \times (N_{x0} \lambda_m^2 + N_{y0} \delta_n^2) W = 0 \end{aligned} \tag{19}$$

4. Closed-form solution

Rectangular plates are generally classified in accordance with the type of support employed. Here, we are concerned with the exact solutions of Eq. (19) for a simply supported FG plate resting on elastic foundation.

4.1 Mechanical buckling

Consider a simply supported rectangular plate resting on elastic foundation with length a and width b which is subjected to in-plane loading in two directions

$$N_{x0} = -F_x h, \quad N_{y0} = -F_y h \tag{20}$$

And Eq. (19) leads to

$$F_x = e_1^1 \frac{W}{h(W)} \tag{21}$$

Where

$$e_1^1 = \frac{(D_1 D_3 - D_2^2)(\lambda_m^2 + \delta_n^2)^3 + D_1 D_4 (\lambda_m^2 + \delta_n^2)^2}{(\lambda_m^2 + \beta\ \delta_n^2)[D_3 (\lambda_m^2 + \delta_n^2) + D_4]} + \frac{[K_w + K_s a^2 (\lambda_m^2 + \delta_n^2)]\ D_c}{a^4 (\lambda_m^2 + \beta\ \delta_n^2)} \tag{22}$$

In which

$$\beta = F_y / F_x \ , \ K_w = \frac{k_w a^4}{D_c} \ , \ K_s = \frac{k_s a^2}{D_c} \tag{23}$$

4.2 Thermal buckling

A rectangular plate under thermal loads is examined in this part. To determine the critical stability temperature, the pre-buckling thermal loads should be found. Thus, solving the membrane form of the equilibrium equations and by employing the method presented by Meyers and Hyer [53], the pre-buckling load resultants of FG plate exposed to the temperature distribution within the thickness are found to be

$$N_{x0} = N_{y0} = -\frac{\Phi_1}{1-\nu} \tag{24}$$

And

$$\begin{aligned}\frac{\Phi_1}{1-\nu} = &\left[\frac{[(D_1D_3 - D_2^2)(\lambda_m^2+\delta_n^2)^2 + D_1D_4(\lambda_m^2+\delta_n^2)]}{D_3(\lambda_m^2+\delta_n^2)+D_4} + \frac{[K_w + K_s a^2(\lambda_m^2+\delta_n^2)]\, D_c}{a^4(\lambda_m^2+\delta_n^2)}\right] \\ &+\left[\frac{E_1\left[(D_3(\lambda_m^4\delta_n^2+\lambda_m^2\delta_n^4+\lambda_m^6+\delta_n^6)+D_4(\lambda_m^4+\delta_n^4))\right]}{16\left[D_3(\lambda_m^2+\delta_n^2)+D_4\right](\lambda_m^2+\delta_n^2)} + \frac{E_1(\lambda_m^4+2\,\nu\,\lambda_m^2\delta_n^2+\delta_n^4)}{8(1-\nu^2)\ (\lambda_m^2+\delta_n^2)}\right] W^2\end{aligned} \tag{25}$$

In this work, to study the influence of assumption type of temperature variation within the thickness on thermal stability behavior of FG plate resting on elastic foundation, three types of thermal loading within the plate thickness are considered.

4.2.1 Uniform temperature rise (UTR)

It is considered that the initial uniform temperature of the FG plate is T_i, and the temperature is uniformly raised to a final value T_f such that the plate buckles. The temperature change $\Delta T = T_f - T_i$ is considered to be independent from thickness variable. The thermal parameter Φ_1 is obtained from Eq. (9b), and substitution of the result into Eq. (25) yields

$$\begin{aligned}\Delta T_{Cr} &= e_1^2 \\ &= \frac{(1-\nu)\left[(D_1D_3 - D_2^2)(\lambda_m^2+\delta_n^2)^2 + D_1D_4(\lambda_m^2+\delta_n^2)\right]}{L\,[D_3(\lambda_m^2+\delta_n^2)+D_4]} + \frac{[K_w + K_s a^2(\lambda_m^2+\delta_n^2)]\, D_c(1-\nu)}{a^4\,L(\lambda_m^2+\delta_n^2)}\end{aligned} \tag{26}$$

Where

$$L = \int_{-h/2}^{h/2} \alpha(z)E(z)dz \tag{27}$$

4.2.2 Linear temperature distribution through the thickness (LTD)

As an approximation, consider the following linear temperature variation along the thickness coordinate of the FG plate as

$$T(z) = \Delta T\left(\frac{z}{h} + \frac{1}{2}\right) + T_m, \quad \Delta T = T_c - T_m \tag{28}$$

Same as UTR procedure, the following expression for thermal buckling load is obtained:

$$\Delta T_{Cr} = e_1^2 - \frac{T_m L}{H} \tag{29}$$

With

$$e_1^2 = \frac{(1-\nu)\left[(D_1 D_3 - D_2^2)(\lambda_m^2 + \delta_n^2)^2 + D_1 D_4 (\lambda_m^2 + \delta_n^2)\right]}{H\,[D_3(\lambda_m^2 + \delta_n^2) + D_4]} + \frac{[K_w + K_s a^2(\lambda_m^2 + \delta_n^2)]\, D_c(1-\nu)}{a^4 H(\lambda_m^2 + \delta_n^2)} \tag{30}$$

and

$$H = \int_{-h/2_1}^{h/2} \alpha(z)\;\; E(z)\left(\frac{z}{h} + \frac{1}{2}\right) dz \tag{31}$$

4.2.3 Non-linear temperature distribution through the thickness (NTD)

The temperature field considered to be uniform over the plate surface but changing along the thickness direction due to heat conduction. In such a case, the temperature variation within the thickness can be determined by solving the steady-state heat transfer equation as

$$\frac{d}{dz}\left[K(z)\frac{dT}{dz}\right] = 0\ ,\ T(z = -h/2) = T_m \quad \text{and} \quad T(z = h/2) = T_c \tag{32}$$

The differential Eq. (32) can be easily solved by employing the polynomial series. Thus, the temperature variation within the plate thickness is determined as

$$T(z) = T_m + \Delta T\ \frac{r\sum_{j=0}^{5} \frac{(-r^N\, K_{cm}/K_m)^j}{jN+1}}{\sum_{j=0}^{5} \frac{(-K_{cm}/K_m)^j}{jN+1}} \tag{33}$$

Where

$$r = \frac{(2z + h)}{2h} \quad \text{and} \quad \Delta T = T_c - T_m \tag{34}$$

Same as UTR procedure, the following expression for thermal buckling load is obtained:

$$\Delta T_{Cr} = e_1^2 - \frac{T_m L}{G} \tag{35}$$

with

$$e_1^2 = \frac{(1-\nu)\left[(D_1 D_3 - D_2^2)(\lambda_m^2 + \delta_n^2)^2 + D_1 D_4 (\lambda_m^2 + \delta_n^2)\right]}{G\,[D_3(\lambda_m^2 + \delta_n^2) + D_4]} + \frac{[K_w + K_s a^2(\lambda_m^2 + \delta_n^2)]\, D_c(1-\nu)}{a^4 G(\lambda_m^2 + \delta_n^2)} \tag{36}$$

And

$$G=\frac{\sum_{j=0}^{5}\frac{(-K_{cm}/K_m)^j}{jN+1}\left[\frac{E_m\alpha_m}{jN+2}+\frac{E_m\alpha_{cm}+E_{cm}\alpha_m}{(j+1)N+2}+\frac{E_{cm}\alpha_{cm}}{(j+2)N+2}\right]}{\sum_{j=0}^{5}\frac{(-K_{cm}/K_m)^j}{jN+1}} \tag{37}$$

5. Numerical results and discussion

In this section, numerical examples are examined and discussed for checking the accuracy of the proposed formulation in determining the mechanical and thermal stability loads. Analytical solutions are determined by employing the Navier solution for simply supported FG plates resting on elastic foundation. Critical buckling loads are determined and the comparison is carried out with the existing results. For numerical results, an Al/Al_2O_3 plate composed of aluminum (as metal) and alumina (as ceramic) is considered. The Young's modulus, thermal conductivity and coefficient of thermal expansion are $E_m = 70$ GPa, $\alpha_m = 23\times10^{-6}/°C$, $K_m = 204$ W/mK and those of alumina are $E_c = 380$ GPa, $\alpha_c = 7.4\times10^{-6}/°C$, $K_c = 10.4$ W/mK, respectively. The Poisson's ratio of the plate is considered to be constant within the thickness and equal to 0.3 [54-56]. For convenience, the following non-dimensional quantities are used in presenting the numerical results in tabular form:

$$K_w=\frac{k_1a^4}{D_c},\ K_s=\frac{k_2a^2}{D_c},\ \hat{N}=\frac{N_{cr}b^2}{D_c},\ \overline{N}=\frac{N_{cr}a^2}{E_mh^3},\ \tilde{N}=\frac{N_{cr}a^2}{\pi^2D_c},\ D_m=\frac{E_mh^3}{12\left(1-\nu^2\right)},\ D_c=\frac{E_ch^3}{12\left(1-\nu^2\right)} \tag{38}$$

5.1 Comparisons for mechanical buckling

Example 1: The non-dimensional critical buckling loads $\tilde{N}$ of simply supported thin homogeneous square plate without or resting on elastic foundations are given in Table 1. The computed results are compared with those reported by Lam et al. [57] based on CPT, Akhavan et al. [58] and Sobhy [59] based on FSDT and Yaghoobi and Fereidoon [56] based on Reddy's theory. It is mentioned that the solutions of Lam et al. [57] are obtained via the Green's function.

Table 1. Comparison of non-dimensional critical buckling load $\tilde{N}$ of a simply supported thin homogeneous square plate resting on elastic foundations $(a/h = 1000)$

Theory	(K_w, K_s)			
	(0,0)	(0,100)	(100,0)	(100,100)
CPT [57]	4.00000	18.92[a]	5.027	19.17[a]
FSDT [58]	3.99998	18.9151[a]	5.02658	19.1717[a]
FSDT [59]	3.99998	18.91506[a]	5.02658	19.17171[a]
HSDT [56]	3.99990	18.91400 [a]	5.02650	19.17200
Present	3.99999	18.91513 [a]	5.02659	19.17178 [a]

[a] Mode for plate is $(m, n) = (2,1)$

Table 2. Comparison of non-dimensional critical buckling load $\widehat{N}$ of a simply supported homogeneous plate under in-plane compression and resting on elastic foundations

a/b	(K_w, K_s)	Theory	a/h			
			5	10	100	1000
0.5	(0,0)	FSDT [58]	54.3207	59.6629	61.6641	61.6848
		FSDT [59]	54.0859	59.5887	61.6633	61.6848
		HSDT [56]	54.0737	59.5856	61.6633	61.6848
		Present	54.0802	59.5871	61.6633	61.6848
	(100,10)	FSDT [58]	144.6952	150.1910	152.1930	152.2130
		FSDT [59]	144.6140	150.1170	152.1920	152.2130
		HSDT [56]	144.6022	150.1141	152.1918	152.2133
		Present	144.6087	150.1156	152.1917	152.2132
	(1000,100)	FSDT [58]	643.5000[b]	686.1710[a]	704.3860[a]	704.5890[a]
		FSDT [59]	641.380[b]	685.567[a]	704.378[a]	704.589[a]
		HSDT [56]	640.9782 [b]	685.5369 [a]	704.3775 [a]	704.5888 [a]
		Present	641.2294[b]	685.5529[a]	704.3776[a]	704.5887[a]
1	(0,0)	FSDT [58]	32.4414	37.4477	39.457	39.4782
		FSDT [59]	32.2398	37.3753	39.4562	39.4782
		HSDT [56]	32.2276	37.3721	39.4562	39.4782
		Present	32.2343	37.3737	39.4561	39.4781
	(100,10)	FSDT [58]	55.0289[a]	67.5798	69.5891	69.6103
		FSDT [59]	54.6116[a]	67.5074	69.5883	69.6103
		HSDT [56]	54.5692 [a]	67.5042	69.5883	69.6103
		Present	54.5945[a]	67.5058	69.5882	69.6103
	(1000,100)	FSDT [58]	174.9760[b]	204.6510 [a]	211.9610 [a]	212.0140 [a]
		FSDT [59]	174.391[b]	204.416 [a]	211.928 [a]	212.014 [a]
		HSDT [56]	174.2676 [b]	204.4040 [a]	211.9285 [a]	212.0145 [a]
		Present	174.3451[b]	204.4105[a]	211.9285[a]	212.0144[a]
2	(0,0)	FSDT [58]	19.2255 [b]	32.4414 [a]	39.3930 [a]	39.4776 [a]
		FSDT [59]	19.0400 [b]	32.2398 [a]	39.3897 [a]	39.4775 [a]
		HSDT [56]	18.9794 [b]	32.2276 [a]	39.3896 [a]	39.4775 [a]
		Present	19.0182[b]	32.2343[a]	39.3896[a]	39.4775[a]
	(100,10)	FSDT [58]	22.7476[c]	37.5182[b]	45.0262 [a]	45.1108 [a]
		FSDT [59]	22.6778[c]	37.8581 [b]	45.0229 [a]	45.1108 [a]
		HSDT [56]	22.5785 [c]	37.8358 [b]	45.0228 [a]	45.1108 [a]
		Present	22.6434[c]	37.8486[b]	45.0228[a]	45.1107[a]
	(1000,100)	FSDT [58]	-	72.8290 [c]	85.0953[b]	85.2563[b]
		FSDT [59]	52.2276[d]	72.4117 [c]	85.0889[b]	85.2562[b]
		HSDT [56]	50.0214 [d]	72.3694 [c]	85.0887 [b]	85.2562 [b]
		Present	50.1233[d]	72.3946[c]	85.0887[b]	85.2562[b]

[a] Mode for plate is (m, n)=(2, 1).
[b] Mode for plate is (m, n)=(3, 1).
[c] Mode for plate is (m, n)=(4, 1).
[d] Mode for plate is (m, n)=(5, 1).

Table 3. Comparison of non-dimensional critical buckling load $\overline{N}$ of a simply supported FG plate resting on elastic foundations (a/b=1, a/h=10)

β	(K_w, K_s)	Theory	N					
			0	0.5	1	2	5	10
0	(0, 0)	HSDT [56]	18.5785	12.1229	9.3391	7.2631	6.0353	5.4528
		Present	18.5793	12.1234	9.3394	7.2627	6.0329	5.4475
	(100, 10)	HSDT [56]	21.3379	14.8823	12.0985	10.0224	8.7947	8.2122
		Present	21.3386	14.8828	12.0987	10.0220	8.7922	8.1992
	(1000, 100)	HSDT [56]	40.6477[a]	31.4605[a]	27.4319[a]	24.3470[a]	22.3602[a]	21.4516[a]
		Present	40.6510[a]	31.4625[a]	27.4333[a]	24.3459[a]	22.3527[a]	21.4341[a]
1	(0, 0)	HSDT [56]	9.2893	6.0615	4.6695	3.6315	3.0177	2.7264
		Present	9.2896	6.0617	4.6697	3.6313	3.0164	2.7168
	(100, 10)	HSDT [56]	10.6689	7.4411	6.0492	5.0112	4.3973	4.1061
		Present	10.6693	7.4414	6.0493	5.0110	4.3961	4.0995
	(1000, 100)	HSDT [56]	23.0860	19.8582	18.4663	17.4283	16.8144	16.5232
		Present	23.0864	19.8584	18.4664	17.4281	16.8132	16.5210

[a] Mode for plate is (m, n)=(2, 1).

Good agreement is observed between the proposed theory and the published ones. Also, Table 2 shows the non-dimensional buckling loads $\widehat{N}$ of simply supported homogeneous plate under uniaxial compression. The computed results are compared with those found by Akhavan et al. [58] and Sobhy [59] based on FSDT and Yaghoobi and Fereidoon [56] based on Reddy's theory. Good agreement can be observed for different values of foundation coefficients, K_w and K_s, aspect ratio a/b, and thickness ratio h/a.

Example 2: Table 3 provide the non-dimensional critical buckling loads $\overline{N}$ of simply supported Al/Al_2O_3 square plate for different values of material index N and foundation parameters K_w and K_s. The predicted non-dimensional critical buckling loads are compared with those reported by Yaghoobi and Fereidoon [56]. In this table, two different loading cases are considered, and six arbitrary values of the material index N are taken. Three combinations of foundation parameters, K_w and K_s are also considered. It can be seen that the results calculated using the present model are in good agreement with those reported by Yaghoobi and Fereidoon [56] for all loading types, material index, and foundation parameters. It should be signaled that in this example the dimensionless foundation coefficients, K_w and K_s are $k_w a^4/D_m$ and $k_s a^2/D_m$ respectively.

Fig. 2 Show the effect of the gradient index on the non-dimensional critical buckling load $\overline{N}$ of a square FG plate resting on elastic foundations. From the obtained graph, we can see that the non-dimensional critical buckling load ($\overline{N}$) is in inverse relation with power index N. The smaller values of $\overline{N}$ are obtained for FG-plate under biaxial compressive load (β=1), the biggest one is when the plate is under uniaxial compression (β=0).

5.2 Comparisons for thermal buckling

The general formulation for the thermal stability analysis of the FG plates subjected to the

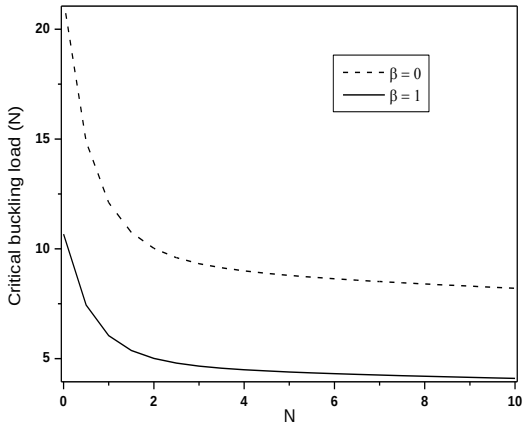

Figure 2. Effect of the gradient index on the non-dimensional critical buckling load $\overline{N}$ of a square FG plate resting on elastic foundations ($a/h = 10, K_w = 100, K_s = 10$)

Table 4. Comparison of critical buckling temperature difference $\Delta T_{cr} \times 10^{-3}$ of square FG plate resting on elastic foundation under UTR

N	Theory	$(K_w, K_s) = (0,0)$		$(K_w, K_s) = (10,0)$		$(K_w, K_s) = (10,10)$	
		$a/h = 5$	$a/h = 10$	$a/h = 5$	$a/h = 10$	$a/h = 5$	$a/h = 10$
0	CPT [60]	6.83964	1.70991	7.01519	1.75380	10.4801	2.62005
	FSDT [61]	5.58069	1.61862	5.75623	1.66251	9.22123	2.52876
	HSDT [56]	5.58344	1.61868	5.75899	1.66257	9.22398	2.52882
	TPT [60]	5.58556	1.61882	5.76109	1.66270	9.22610	2.52896
	Present	5.58461	1.61875	5.76015	1.66263	9.22515	2.52888
1	CPT [60]	3.17751	0.79438	3.34112	0.83528	6.57068	1.64267
	FSDT [61]	2.67039	0.75837	2.83400	0.79928	6.06356	1.60667
	HSDT [56]	2.67153	0.75840	2.83515	0.79930	6.06470	1.60669
	TPT [60]	2.67241	0.75845	2.83603	0.79935	6.06558	1.60674
	Present	2.67201	0.75842	2.83562	0.79932	6.06519	1.60671
5	CPT [60]	2.90629	0.72657	3.13305	0.78326	7.60938	1.90234
	FSDT [61]	2.35948	0.68678	2.58625	0.74347	7.06257	1.86255
	HSDT [56]	2.27501	0.67931	2.50179	0.73600	6.97810	1.85508
	TPT [60]	2.27131	0.67895	2.49808	0.73564	6.97440	1.85472
	Present	2.27221	0.67903	2.49898	0.73573	6.97530	1.85481
10	CPT [60]	2.98770	0.74693	3.24365	0.81091	8.29575	2.07394
	FSDT [61]	2.36822	0.70108	2.62416	0.76507	7.67626	2.02809
	HSDT [56]	2.27678	0.69269	2.53273	0.75668	7.58483	2.01970
	TPT [60]	2.27551	0.69254	2.53146	0.75653	7.58356	2.01955
	Present	2.24045	0.69133	2.53163	0.75655	7.58372	2.01957

uniform, linear and nonlinear temperature rises through-the-thickness is examined here. Tables 4-6 provide the critical stability temperature difference ($\Delta T_{Cr} \times 10^{-3}$) for FG plates subjected to the uniform, linear and nonlinear temperature distribution through the thickness, respectively.

Table 5. Comparison of critical buckling temperature difference $\Delta T_{Cr} \times 10^{-3}$of square FG plate resting on elastic foundation under LTD

N	Theory	$(K_w, K_s) = (0,0)$		$(K_w, K_s) = (10,0)$		$(K_w, K_s) = (10,10)$	
		$a/h = 5$	$a/h = 10$	$a/h = 5$	$a/h = 10$	$a/h = 5$	$a/h = 10$
0	CPT [60]	13.66929	3.40982	14.02036	3.49759	20.95037	5.23009
	FSDT [61]	11.15138	3.22725	11.50246	3.31502	18.43246	5.04752
	HSDT [56]	11.15688	3.22736	11.50796	3.31513	18.43797	5.04764
	TPT [60]	11.16112	3.22764	11.51220	3.31541	18.44220	5.04791
	Present	11.15922	3.22750	11.51030	3.31527	18.44031	5.04777
1	CPT [60]	5.94993	1.48045	6.25678	1.55716	12.31372	3.07140
	FSDT [61]	4.99885	1.41292	5.30570	1.48964	11.36263	3.00387
	HSDT [56]	5.00099	1.41297	5.30784	1.48968	11.36477	3.00391
	TPT [60]	5.00264	1.41307	5.30948	1.48978	11.36642	3.00402
	Present	5.00190	1.41302	5.30874	1.48973	11.36568	3.00396
5	CPT [60]	4.99396	1.24204	5.38430	1.33962	13.08936	3.26588
	FSDT [61]	4.05274	1.17354	4.44308	1.27113	12.14814	3.19739
	HSDT [56]	3.90735	1.16069	4.29770	1.25827	12.00275	3.18453
	TPT [60]	3.90098	1.16006	4.29132	1.25765	11.99637	3.18391
	Present	3.90254	1.16021	4.29288	1.25780	11.99794	3.18406
10	CPT [60]	5.28555	1.31474	5.73910	1.42813	14.69174	3.66629
	FSDT [61]	4.18778	1.23350	4.64132	1.34688	13.59396	3.58504
	HSDT [56]	4.02576	1.21864	4.47930	1.33203	13.43194	3.57019
	TPT [60]	4.02350	1.21837	4.47705	1.33176	13.42969	3.56992
	Present	4.02381	1.21841	4.47735	1.33180	13.43104	3.56850

5.2.1 Uniform temperature rise (UTR)

The buckling temperature difference $\Delta T_{Cr} \times 10^{-3}$ of simply supported thick homogeneous square plate without or resting on elastic foundations square FG plate resting on elastic foundation under UTR is given in Table 4. The computed results are compared with those reported by Zenkour and Sobhy [60] based on CPT, Yaghoobi and Torabi [61] based on FSDT and Yaghoobi and Fereidoon [56] based on Reddy's theory, Zenkour and Sobhy [60] based on TPT. The examination of this table demonstrates that the results provided by the present analytical method are in a good agreement with those reported by by Zenkour and Sobhy [60]. Good agreement can be observed for different values of foundation coefficients, K_w and K_s, and thickness ratio a/h.

5.2.2 Linear temperature distribution through the thickness (LTD)

In order to verify the validity of the proposed method in predicting the thermal buckling behaviors of plates under LTD, a comparison has been performed with the results reported by Zenkour and Sobhy [60] based on CPT, Yaghoobi and Torabi [61] based on FSDT and based on Reddy's theory, Zenkour and Sobhy [60] based on TPT. The critical buckling temperature difference $\Delta T_{Cr} \times 10^{-3}$ of simply supported thick homogeneous square plate without or resting on elastic foundations has been given in Table 5. For the present material properties, the critical buckling temperatures decrease rapidly within the range of N=0 (ceramic rich) to N=5. As the

Table 6. Comparison of critical buckling temperature difference $\Delta T_{Cr} \times 10^{-3}$ of square FG plate resting on elastic foundation under NTD

N	Theory	$(K_w, K_s) = (0,0)$		$(K_w, K_s) = (10,0)$		$(K_w, K_s) = (10,10)$	
		$a/h = 5$	$a/h = 10$	$a/h = 5$	$a/h = 10$	$a/h = 5$	$a/h = 10$
0	CPT [60]	13.66929	3.40982	14.02036	3.49759	20.95037	5.23009
	FSDT [61]	11.15138	3.22725	11.50246	3.31502	18.43246	5.04752
	HSDT [56]	11.15688	3.22736	11.50796	3.31513	18.43797	5.04764
	TPT [60]	11.16112	3.22764	11.51220	3.31541	18.44220	5.04791
	Present	11.16922	3.22750	11.51030	3.31527	18.44031	4.04777
1	CPT [60]	8.25905	2.05500	8.68499	2.16148	17.09257	4.26338
	FSDT [61]	6.93886	1.96127	7.36479	2.06775	15.77238	4.16965
	HSDT [56]	6.94183	1.96133	7.36777	2.06781	15.77535	4.16971
	TPT [60]	6.94412	1.96147	7.37005	2.06796	15.77763	4.16985
	Present	6.94309	1.96140	7.36903	2.06788	15.77661	4.16978
5	CPT [60]	6.24563	1.55334	6.73381	1.67538	16.37004	4.08444
	FSDT [61]	5.06851	1.46768	5.55669	1.58972	15.19291	3.99878
	HSDT [56]	4.88668	1.45160	5.37486	1.57364	15.01109	3.98270
	TPT [60]	4.87871	1.45082	5.36688	1.57286	15.00311	3.98192
	Present	4.88065	1.45101	5.36883	1.57305	15.00050	3.98211
10	CPT [60]	6.10899	1.51957	6.63320	1.65062	16.98057	4.23746
	FSDT [61]	4.84020	1.42567	5.36440	1.55672	15.71178	4.14356
	HSDT [56]	4.65293	1.40849	5.17714	1.53954	15.52451	4.12639
	TPT [60]	4.65033	1.40818	5.17453	1.53923	15.52191	4.12608
	Present	4.65068	1.40823	5.17488	1.53928	15.52226	4.12613

power law index N becomes larger, all the critical buckling temperatures approach slowly to the values for N=10 (metallic rich).

5.2.3 Non-linear temperature distribution through the thickness (NTD)

To check also the validity of the proposed formulation, another comparative study for evaluation of critical buckling temperatures between the presented theory and analytical solutions developed by Zenkour and Sobhy [60] based on CPT, Yaghoobi and Torabi [61] based on FSDT and Yaghoobi and Fereidoon [56] based on Reddy's theory, Zenkour and Sobhy [60] based on TPT. The effect of foundation stiffness on the thermal buckling behavior of FG plates subjected to uniaxial compression is presented in Table 6. As expected, the foundation stiffness increases the critical buckling temperature difference $\Delta T_{Cr} \times 10^{-3}$ of FG plate. From the results, it can be also seen that there is a very good agreement between the present formulation and the TPT theory proposed by Zenkour and Sobhy [60].

Fig. 3 shows the effect of the side-to-thickness ratio a/h on the ΔT_{Cr} of a square FG plate resting on elastic foundations for all three types of thermal loads (UTR, LTD, NTD). As indicated, the critical buckling temperature difference ΔT_{Cr} decreases gradually with the increase of the side-to-thickness ratio a/h wherever the loading type is. The critical buckling temperature difference ΔT_{Cr} will be maximum for NTD and minimum for UTR.

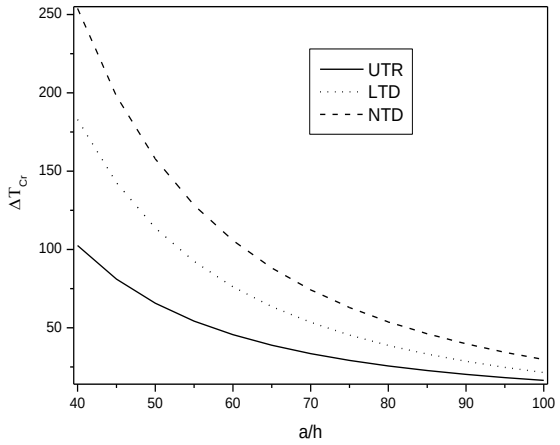

Figure 3. Effect of the side-to-thickness ratio on the ΔT_{Cr} of a square FG plate resting on elastic foundations ($N = 1, K_w = 100, K_s = 10$)

Finally, the present comparative studies show that the results obtained from the proposed method agree well with existing analytical results in the literature which validate the reliability and accuracy of the present analytical approach. It should be noted that the proposed innovative HSDT and Airy stress function method involves four unknowns as against five in case of conventional FSDT and HSDT.

6. Conclusions

In this study, the mechanical and thermal buckling analysis of thick functionally graded (FG) plates resting on elastic foundations was investigated using an innovative higher-order shear deformation theory (HSDT) combined with the Airy stress function method.

- For mechanical buckling, the P-FG plate was subjected to uniaxial and biaxial in-plane compressive loads, while three types of thermal loading (uniform, linear, and nonlinear temperature rise through the thickness) were considered for thermal buckling analysis.
- The effects of key parameters such as the power-law index, foundation stiffness, loading conditions, and plate thickness ratio on the critical buckling loads and temperatures were thoroughly examined.
- The accuracy and efficiency of the proposed model were validated through comprehensive comparisons with existing results from the literature obtained using various plate theories.
- It is concluded that the present formulation based on the Airy stress function provides an efficient and accurate tool for predicting the critical mechanical and thermal buckling responses of FG plates. The model significantly reduces the number of unknowns, leading to lower computational cost while maintaining high accuracy, and can be extended to analyze other advanced composite structures.

Finally, future research will focus on extending the proposed innovative HSDT and Airy stress function approach to more complex problems, including post-buckling behavior, dynamic analysis under various loading conditions, FG plates with porosities or reinforced by graphene platelets, as well as plates with different boundary conditions and resting on nonlinear elastic foundations.

References

1. Esen, I. (2019). Dynamic response of a functionally graded Timoshenko beam on two-parameter elastic foundations due to a variable velocity moving mass. International Journal of Mechanical Sciences, 153, 21-35. https://doi.org/10.1016/j.ijmecsci.2019.01.033.
2. Elmascri, S., Bessaim, A., Taleb, O., Houari, M.S.A., Mohamed, S., Bernard, F., Tounsi, A. (2020). A novel hyperbolic plate theory including stretching effect for free vibration analysis of advanced composite plates in thermal environments. Structural Engineering and Mechanics, 75(2), 193-209. https://doi.org/10.12989/sem.2020.75.2.193.
3. Bezzina, S., Bessaim, A., Houari, M.S.A., Azab, M. (2022). A new quasi-3D plate theory for free vibration analysis of advanced composite nanoplates. Steel and Composite Structures, 45(13), 839-850. https://doi.org/10.12989/sss.2022.45.6.839.
4. Wei, Y.Y., Al-Furjan, M.S.H., Shan, L., Shen, X., Kolahchi, R., Rabani Bidgoli, M., Farrokhian, A. (2024). Micro-mass sensor-based vibration response of smart bidirectional functionally graded auxetic microbeams. Archives of Civil and Mechanical Engineering, 24(1), 38. https://doi.org/10.1007/s43452-023-00840-2.
5. Belarbi, M.O., Benounas, S., Salami, S.J., Khechai, A., Daikh, A.A., Houari, M.S.A., Bezzina, S. (2025). An enhanced finite element model for static bending analysis of functionally graded plates with power-law, exponential, and sigmoid material gradients. Archive of Applied Mechanics, 95(1), 1-24. https://doi.org/10.1007/s00419-024-02727-x.
6. Uysal, M.U. (2016). Buckling behaviours of functionally graded polymeric thin-walled hemispherical shells. Steel and Composite Structures, 21(4), 849-862. https://doi.org/10.12989/scs.2016.21.4.849.
7. Esen, I., Abdelrahman, A.A., Eltaher, M.A. (2021). On vibration of sigmoid/symmetric functionally graded nonlocal strain gradient nanobeams under moving load. International Journal of Mechanics and Materials in Design, 17(3), 721-742. https://doi.org/10.1007/s00707-023-03722-z.
8. Daikh, A.A. (2020). Thermal buckling analysis of functionally graded sandwich cylindrical shells. Advances in Aircraft and Spacecraft Science, 7(4), 335-351. https://doi.org/10.12989/aas.2020.7.4.335.
9. Garg, A., Chalak, H.D., Zenkour, A.M., Belarbi, M.O., Houari, M.S.A. (2022). A review of available theories and methodologies for the analysis of nano isotropic, nano functionally graded, and CNT reinforced nanocomposite structures. Archives of Computational Methods in Engineering, 1-34. https://doi.org/10.1007/s11831-021-09652-0.
10. Belarbi, M.O., Khechai, A., Houari, M.S.A., Bessaim, A., Hirane, H., Garg, A. (2024). Free vibration behavior of sandwich FGM beams: parametric and uncertainty analysis. Journal of Vibration Engineering & Technologies, 12(Suppl 1), 883-905. https://doi.org/10.1007/s42417-024-01452-7.
11. Yıldırım, E., Esen, I. (2024). Effect of the porous structure on the hygrothermal vibration analysis of functional graded nanoplates using nonlocal high-order continuum plate model. Acta Mechanica, 235(8), 5079-5106. https://doi.org/10.1007/s00419-025-02793-9.
12. Meski, K., Esen, I., Menasria, A., Bouhadra, A., Mamen, B., Tounsi, A., ... Khedher, K.M. (2025). Elastic instability of functionally graded sandwich plates with auxetic honeycomb core subjected to thermal and magnetic fields. International Journal of Structural Stability and Dynamics, 2650272. https://doi.org/10.1142/S021945542650272X.
13. Buğday, M., Esen, I. (2025). Investigation of 3D wave propagation in foam-core functionally graded material magneto-piezoelectric smart nanoplates. Advanced Engineering Materials, 27(16), 2500436. https://doi.org/10.1002/adem.202500436.
14. Daikh, A.A., Houari, M.S.A., Belarbi, M.O., Mohamed, S.A., Eltaher, M.A. (2022). Static and dynamic stability responses of multilayer functionally graded carbon nanotubes reinforced composite nanoplates via quasi 3D nonlocal strain gradient theory. Defence Technology, 18(10), 1778-1809. https://doi.org/10.1016/j.dt.2021.09.011.
15. Daikh, A.A., Belarbi, M.O., Ahmed, D., Houari, M.S.A., Avcar, M., Tounsi, A., Eltaher, M.A. (2023). Static analysis of functionally graded plate structures resting on variable elastic foundation under

various boundary conditions. Acta Mechanica, 234(2), 775-806. https://doi.org/10.1007/s00707-022-03405-1.

16. Remil, A., Belarbi, M.O., Bessaim, A., Houari, M.S.A., Bouamoud, A., Daikh, A.A., ... Eltaher, M.A. (2023). An accurate analytical model for the buckling analysis of FG-CNT reinforced composite beams resting on an elastic foundation with arbitrary boundary conditions. Computers and Concrete, 31(3), 267-276. https://doi.org/10.12989/cac.2023.31.3.267.
17. Cho, J.R. (2022). Thermal buckling analysis of metal-ceramic functionally graded plates by natural element method. Structural Engineering and Mechanics, 84(6), 723-731. https://doi.org/10.12989/sem.2022.84.6.723.
18. Alnujaie, A., Sayyad, A.S., Hadji, L., Tounsi, A. (2022). Buckling and free vibration analysis of multi-directional functionally graded sandwich plates. Structural Engineering and Mechanics, 84(6), 813-822. https://doi.org/10.12989/sem.2022.84.6.813.
19. Drai, A., Daikh, A.A., Belarbi, M.O., Houari, M.S.A., Aour, B., Hamdi, A., Eltaher, M.A. (2023). Bending of axially functionally graded carbon nanotubes reinforced composite nanobeams. Advances in Nano Research, 14(3), 211-224. https://doi.org/10.12989/anr.2023.14.3.211.
20. Djedid, I.K., Yahia, S.A., Draiche, K., Madenci, E., Benrahou, K.H., Tounsi, A. (2024). A new four-unknown equivalent single layer refined plate model for buckling analysis of functionally graded rectangular plates. Structural Engineering and Mechanics, 90(5), 517-530. https://doi.org/10.12989/sem.2024.90.5.517.
21. Turan, M., Adiyaman, G. (2024). Free vibration and buckling analysis of porous two-directional functionally graded beams using a higher-order finite element model. Journal of Vibration Engineering & Technologies, 12(1), 1133-1152. https://doi.org/10.1007/s42417-023-00898-5.
22. Ermis, M., Dorduncu, M., Kutlu, A. (2024). Peridynamic differential operator for stress analysis of imperfect functionally graded porous sandwich beams based on refined zigzag theory. Applied Mathematical Modelling, 133, 414-435. https://doi.org/10.1016/j.apm.2024.05.032.
23. Xin, L., Kiani, Y. (2023). Vibration characteristics of arbitrary thick sandwich beam with metal foam core resting on elastic medium. Structures, 49, 1-11. https://doi.org/10.1016/j.istruc.2023.01.108.
24. Kant, T. (1993). A critical review and some results of recently developed refined theories of fiber-reinforced laminated composites and sandwiches. Composite Structures, 23(4), 293-312. https://doi.org/10.1016/0263-8223(93)90230-N.
25. Kant, T., Swaminathan, K. (2001). Free vibration of isotropic, orthotropic, and multilayer plates based on higher order refined theories. Journal of Sound and Vibration, 241(2), 319-327. https://doi.org/10.1006/jsvi.2000.3232.
26. Javaheri, R., Eslami, M. (2002a). Thermal buckling of functionally graded plates. AIAA Journal, 40(1), 162-169. https://doi.org/10.2514/2.1626.
27. Shariat, B.S., Eslami, M.R. (2006). Thermal buckling of imperfect functionally graded plates. International Journal of Solids and Structures, 43(14-15), 4082-4096. https://doi.org/10.1016/j.ijsolstr.2005.04.005.
28. Kazerouni, S.M., Saidi, A.R., Mohammadi, M. (2010). Buckling analysis of thin functionally graded rectangulare plates with two opposite edges simply supported. International Journal of Engineering Transactions B: Applications, 23, 179-192.
29. Kiani, Y., Bagherizadeh, E., Eslami, M.R. (2011). Thermal buckling of clamped thin rectangular FGM plates resting on Pasternak elastic foundation (Three approximate analytical solutions). ZAMM-Journal of Applied Mathematics and Mechanics/Zeitschrift für Angewandte Mathematik und Mechanik, 91(7), 581-593. https://doi.org/10.1002/zamm.201000184.
30. Xing, Y., Wang, Z. (2017). Closed form solutions for thermal buckling of functionally graded rectangular thin plates. Applied Sciences, 7(12), 1256. https://doi.org/10.3390/app7121256.
31. Sitli, Y., Mhada, K., Bourihane, O., Rhanim, H. (2021). Buckling and post-buckling analysis of a functionally graded material (FGM) plate by the asymptotic numerical method. Structures, 31, 1031-1040. https://doi.org/10.1016/j.istruc.2021.01.100.
32. Trabelsi, S., Frikha, A., Zghal, S., Dammak, F. (2018). Thermal post-buckling analysis of functionally

graded material structures using a modified FSDT. International Journal of Mechanical Sciences, 144, 74-89. https://doi.org/10.1016/j.ijmecsci.2018.05.033.

33. Fekrar, A., Tounsi, A., El Meiche, N., Bessaim, A., Bedia, E.A. (2012). Buckling analysis of functionally graded hybrid composite plates using a new four variable refined plate theory. Steel and Composite Structures, 13(1), 91-107. https://doi.org/10.12989/scs.2012.13.1.091.
34. Kettaf, F.Z., Houari, M.S.A., Benguediab, M., Tounsi, A. (2013). Thermal buckling of functionally graded sandwich plates using a new hyperbolic shear displacement model. Steel and Composite Structures, 15(4), 399-423. https://doi.org/10.12989/scs.2013.15.4.399.
35. Zenkour, A.M., Aljadani, M.H. (2018). Mechanical buckling of functionally graded plates using a refined higher-order shear and normal deformation plate theory. Advances in Aircraft and Spacecraft Science, 5(6), 615. https://doi.org/10.12989/aas.2018.5.6.615.
36. Shanab, R., Mohamed, S., Tharwan, M.Y., Assie, A.E., Eltaher, M.A. (2022). Buckling of 2D FG Porous unified shear plates resting on elastic foundation based on neutral axis. Steel and Composite Structures, 45(5), 729-747. https://doi.org/10.12989/scs.2022.45.5.729.
37. Li, Y.P., She, G.L., Gan, L.L., Liu, H.B. (2023). Nonlinear thermal post-buckling analysis of graphene platelets reinforced metal foams plates with initial geometrical imperfection. Steel and Composite Structures, 46(5), 649-658. https://doi.org/10.12989/scs.2023.46.5.649.
38. Tamrabet, A., Mamen, B., Menasria, A., Bouhadra, A., Tounsi, A., Ghazwani, M.H., ... Mahmoud, S.R. (2023). Buckling behaviors of FG porous sandwich plates with metallic foam cores resting on elastic foundation. Structural Engineering and Mechanics, 85(3), 289-304. https://doi.org/10.12989/sem.2023.85.3.289.
39. Lekouara, L., Mamen, B., Bouhadra, A., Menasria, A., Benrahou, K.H., Tounsi, A., Al-Osta, M.A. (2023). Theoretical buckling analysis of inhomogeneous plates under various thermal gradients and boundary conditions. Structural Engineering and Mechanics, 86(4), 443-459. https://doi.org/10.12989/sem.2023.86.4.443.
40. Hadji, L., Madan, R., Atmane, H.A., Bernard, F., Zouatnia, N., Safa, A. (2024). Thermal buckling Analysis of functionally graded plates using trigonometric shear deformation theory for temperature-dependent material properties. Structural Engineering and Mechanics, 91(6), 539-549. https://doi.org/10.12989/sem.2024.91.6.539.
41. Gao, X.Y., Wang, Z.Z., Ma, L.S. (2024). Bending and buckling analysis of functionally graded graphene platelets reinforced composite plates supported by local elastic foundations based on simple refined plate theory. Archive of Applied Mechanics, 94(8), 2123-2150. https://doi.org/10.1007/s00419-024-02629-y.
42. Gholami, R., Ansari, R., Aghdasi, P., Sahmani, S. (2025). Buckling and postbuckling of embedded sandwich moderately thick plates with functionally graded graphene nanoplatelet-reinforced porous core and metallic face sheets. Thin-Walled Structures, 210, 113063. https://doi.org/10.1016/j.tws.2025.113063.
43. Aljadani, M.H. (2024). The porosity effect on the buckling analysis of functionally graded plates under thermal environment using a Quasi-3D theory. Scientific Reports, 14(1), 1-21. https://doi.org/10.1038/s41598-024-79894-y.
44. Chenafi, M., Bourezane, M., Assas, T., Tati, A. (2025). A novel strain-based approach with high-order shear deformation for enhanced static and buckling performance of functionally graded plates. Mechanics of Advanced Materials and Structures, 1-20. https://doi.org/10.1080/15376494.2025.2473687.
45. Houari, M.S.A., Bessaim, A., Bezzina, S., Tounsi, A., Daikh, A.A., Garg, A., Belarbi, M.O. (2024). Thermoelastic bending analysis of thick functionally graded sandwich plates with arbitrary graded material properties using a novel quasi-3D HSDT. Archives of Civil and Mechanical Engineering, 24(2), 80. https://doi.org/10.1007/s43452-024-00898-6.
46. Praveen, G.N., Reddy, J.N. (1998). Nonlinear transient thermoelastic analysis of functionally graded ceramic-metal plates. International Journal of Solids and Structures, 35(33), 4457-4476. https://doi.org/10.1016/S0020-7683(97)00253-9.

47. Abdelrahman, W.G. (2020). Effect of material transverse distribution profile on buckling of thick functionally graded material plates according to TSDT. Structural Engineering and Mechanics, 74(1), 83-90. https://doi.org/10.12989/sem.2020.74.1.083.
48. Tu, T.M., Quoc, T.H., Long, N.V. (2017). Bending analysis of functionally graded plates using new eight-unknown higher order shear deformation theory. Structural Engineering and Mechanics, 62(3), 311-324. https://doi.org/10.12989/sem.2017.62.3.311.
49. Esen, İ., Koç, M.A., Eroğlu, M. (2024). Effect of functionally graded carbon nanotube reinforcement on the dynamic response of composite beams subjected to a moving charge. Journal of Vibration Engineering & Technologies, 12(3), 5203-5218. https://doi.org/10.1080/15376494.2024.2349966.
50. Nguyen, T.K. (2015). A higher-order hyperbolic shear deformation plate model for analysis of functionally graded materials. International Journal of Mechanics and Materials in Design, 11(2), 203-219. https://doi.org/10.1007/s10999-014-9260-3.
51. Librescu, L., Lin, W. (1997). Postbuckling and vibration of shear deformable flat and curved panels on a non-linear elastic foundation. International Journal of Non-linear Mechanics, 32(2), 211-225. https://doi.org/10.1016/S0020-7462(96)00057-1.
52. Lin, W., Librescu, L. (1998). Thermomechanical postbuckling of geometrically imperfect shear–deformable flat and curved panels on a nonlinear elastic foundation. International Journal of Engineering Science, 36(2), 189-206. https://doi.org/10.1016/S0020-7225(97)00055-4.
53. Meyers, C.A., Hyer, M.W. (1991). Thermal buckling and postbuckling of symmetrically laminated composite plates. Journal of Thermal Stresses, 14(4), 519-540. https://doi.org/10.1080/01495739108927083.
54. Javaheri, R., Eslami, M.R. (2002b). Thermal buckling of functionally graded plates based on higher order theory. Journal of Thermal Stresses, 25(7), 603-625. https://doi.org/10.1080/01495730290074333.
55. Lanhe, W. (2004). Thermal buckling of a simply supported moderately thick rectangular FGM plate. Composite Structures, 64(2), 211-218. https://doi.org/10.1016/j.compstruct.2003.08.004.
56. Yaghoobi, H., Fereidoon, A. (2014). Mechanical and thermal buckling analysis of functionally graded plates resting on elastic foundations: an assessment of a simple refined nth-order shear deformation theory. Composites Part B: Engineering, 62, 54-64. https://doi.org/10.1016/j.compositesb.2014.02.014.
57. Lam, K.Y., Wang, C.M., He, X.Q. (2000). Canonical exact solutions for Levy-plates on two-parameter foundation using Green's functions. Engineering Structures, 22(4), 364-378. https://doi.org/10.1016/S0141-0296(98)00116-3.
58. Akhavan, H., Hashemi, S.H., Taher, H.R.D., Alibeigloo, A., Vahabi, S. (2009). Exact solutions for rectangular Mindlin plates under in-plane loads resting on Pasternak elastic foundation. Part II: frequency analysis. Computational Materials Science, 44(3), 951-961. https://doi.org/10.1016/j.commatsci.2008.07.001.
59. Sobhy, M. (2013). Buckling and free vibration of exponentially graded sandwich plates resting on elastic foundations under various boundary conditions. Composite Structures, 99, 76-87. https://doi.org/10.1016/j.compstruct.2012.11.018.
60. Zenkour, A.M., Sobhy, M. (2011). Thermal buckling of functionally graded plates resting_on elastic foundations using the trigonometric theory. Journal of Thermal Stresses, 34, 1119-1138. https://doi.org/10.1080/01495739.2011.606017.
61. Yaghoobi, H., Torabi, M. (2013). Exact solution for thermal buckling of functionally graded plates resting on elastic foundations with various boundary conditions. Journal of Thermal Stresses, 36(9), 869-894. https://doi.org/10.1080/01495739.2013.770356.